Martell, A. E., & Smith, R. M. (1974) *Critical Stability Constants*, Plenum Press, New York.
Martin, R. B., Savory, J., Brown, S., Bertholf, R. L., & Wills, M. R. (1987) *Clin. Chem. 33*, 405-407.
Nakai, C., & Glinsmann, W. (1977) *Biochemistry 16*, 5636-5640.
O'Hara, P. B., & Bersohn, R. (1982) *Biochemistry 21*, 5269-5272.
Penner, M. H., Osuga, D. T., Meares, C. F., & Feeney, R. E. (1987) *Arch. Biochem. Biophys. 252*, 7-14.
Phillips, J. L., & Azari, P. (1972) *Arch. Biochem. Biophys. 151*, 445-452.
Rogers, T. B., Feeney, R. E., & Meares, C. F. (1977) *J. Biol. Chem. 252*, 8108-8112.
Thompson, C. P., McCarty, B. M., & Chasteen, N. D. (1986a) *Biochim. Biophys. Acta 870*, 530-537.
Thompson, C. P., Grady, J. K., & Chasteen, N. D. (1986b) *J. Biol. Chem. 261*, 13128-13134.
Williams, J., Chasteen, N. D., & Moreton, K. (1982) *Biochem. J. 201*, 527-532.
Zweier, J. L. (1978) *J. Biol. Chem. 253*, 7616-7621.

Investigation of the Solution Structure of the Human Parathyroid Hormone Fragment (1-34) by ^{1}H NMR Spectroscopy, Distance Geometry, and Molecular Dynamics Calculations†

Werner Klaus,‡ Thorsten Dieckmann,§ Victor Wray, and Dietmar Schomburg*

Department of Molecular Structure Research, Gesellschaft für Biotechnologische Forschung, Mascheroder Weg 1, D-3300 Braunschweig, Germany

Edgar Wingender and Hubert Mayer

Department of Genetics, Gesellschaft für Biotechnologische Forschung, Mascheroder Weg 1, D-3300 Braunschweig, Germany

Received December 19, 1990; Revised Manuscript Received March 22, 1991

ABSTRACT: The structure of human parathyroid hormone fragment (1-34) in a solvent mixture of water and trifluoroethanol has been determined by ^{1}H nuclear magnetic resonance spectroscopy and a combination of distance geometry and molecular dynamic simulations. After complete assignment of the ^{1}H signals, the nuclear Overhauser enhancement data imply the existence of two α-helices, comprising residues 3-9 and 17-28, joined by a nonstructured region. The absence of any long-range NOEs and the relative magnitudes of the sequential NOEs and the $^3J(H_NH_\alpha)$ values reflect an inherent flexibility within the entire fragment. The final structures refined by molecular dynamics further support the above results and allow discussion of structural-activity relationships.

Parathyroid hormone (PTH)[1] is a peptide hormone of 84 amino acid residues. It regulates the calcium homeostasis in the serum by stimulation of calcium resorption in the kidney and by enhancing resorption of calcified bone matrix. In addition, it also stimulates bone-forming processes. This pleiotropic function is reflected in the identification of at least two different functional domains within the PTH molecule. One of these is located in the amino-terminal region comprising 27 amino acid residues that binds to the PTH receptor(s) and leads to an increased intercellular cAMP synthesis [for review, see Potts et al. (1982)]. These events appear to be involved in bone catabolic effects (Martz et al., 1983; Herrmann-Erlee et al., 1988; Dewhirst et al., 1990). The other functional domain, whose core is at positions 30-34, stimulates DNA synthesis and subsequent cell proliferation of either chondrocytes (Schlüter et al., 1989) or osteoblasts (Sömjen et al., 1990, 1991) via an as yet unidentified cAMP-independent signal transduction pathway.

A study of whether these functional domains also correspond to structural domains is of obvious interest. Unfortunately detailed structural information on the PTH molecule is not available. Conclusions from dark field electron microscopic investigations of bPTH(1-84) suggest the presence of two globular units located within the amino and carboxyl termini, respectively (Fiskin et al., 1977). Similar models have been derived from theoretical considerations on bPTH(1-84) (Zull et al., 1980) as well as from NMR studies that focused on the pH-dependent shifts of the H2 protons of the three histidine moieties in the bovine PTH fragment (1-34) that implied substantial structure for the hormone in solution (Zull et al., 1987; Smith et al., 1987; Coddington et al., 1989). Other ^{1}H NMR investigations, however, have suggested some regular

† This work was part of the "Diplomarbeit" of Thorsten Dieckmann at the University of Braunschweig, Germany (1990).

‡ Present address: F. Hoffmann-LaRoche Ltd., Central Research Unit, Building 65, CH-4002 Basel, Switzerland.

§ Present address: Max-Planck-Institut für Biochemie, D-8033 Martinsried bei München, Germany.

[1] Abbreviations: bPTH, bovine parathyroid hormone; CD, circular dichroism; COSY, correlation spectroscopy; DQF, double-quantum filter; hPTH, human parathyroid hormone; NMR, nuclear magnetic resonance; NOE, nuclear Overhauser enhancement; NOESY, nuclear Overhauser and exchange spectroscopy; RMS, root mean square; TFE, trifluoroethanol; TMS, tetramethylsilane; TOCSY, total correlation spectroscopy.

0006-2960/91/0430-6936$02.50/0

structure at residues 20–24 (Bundi et al., 1976, 1978) although, more recently, neither secondary nor tertiary structure elements for human PTH fragment (1–34) in aqueous solution could be detected (Lee & Russell, 1989). Thus, limited and even contradictory experimental data are available concerning the secondary structure within the PTH fragment (1–34). On the other hand, the structure of this fragment is of great interest in the context of understanding the physiological roles of the hormone, as the fragment displays full activity for both described functions [compare e.g., Potts et al. (1982)]. In this paper, we present direct, unambiguous evidence that, under certain solvent conditions, segments of the hPTH fragment (1–34) adopt α-helical structure whereas other parts do not.

Materials and Methods

Secondary Structure Prediction. The theoretical prediction of α-helices, β-sheets, and turns was performed by using the Robson-directional option within the GENMON program package (Garnier et al., 1978; Lincoln et al., 1990).

Sample Preparation and NMR Spectroscopy. Human PTH fragment 1–34 was purchased from Bachem AG (Bubendorf, Switzerland) and used without further purification. Samples for the 1D NMR experiments consisted of 1 mg of peptide dissolved in 0.5 mL of 100% D_2O or 90% H_2O/10% D_2O, 100 mM phosphate puffer, pH 5.0, to which specific amounts of trifluoroethanol-d_3 (Merck, Darmstadt, Germany) were added as discussed below. For the 2D measurements, 4 mg of the peptide were used in the same solvents. All spectra were referenced to the residual signal of the methylene protons of trifluoroethanol at 3.88 ppm relative to TMS.

^{1}H NMR spectra were recorded at 300 or 308 K on a Bruker AM 600 NMR spectrometer using a dedicated 5-mm proton probe head and an external temperature control (Haake GmbH, Karlsruhe, Germany). All 2D experiments [COSY (Marion & Wüthrich, 1983), COSY-DQF (Rance et al., 1983), TOCSY (Bax & Davis, 1985; Davis & Bax, 1985), and NOESY (Jeener et al., 1979; Macura et al., 1981)] were carried out in the phase-sensitive mode with time-proportional phase increments (Redfield & Kunz, 1975). The signal of the water resonance line was suppressed by low-power irradiation during the relaxation delay (typically 1.3 s) and during the mixing time of the NOESY experiments, by using O1/O2 phase coherence (Zuiderweg et al., 1986). 2D TOCSY spectra were acquired in the "CLEAN" mode (Griesinger et al., 1988) with the MLEV-17 mixing sequence, but without the trim pulses. Total mixing times were 50.3 ms for measurements in the fully deuterated solvents and 75 and 80.7 ms for "H_2O". The corresponding mixing times for the NOESY spectra were 300 ms, or 250 and 350 ms, respectively. Usually, 512 t_1 increments were sampled with 2K data points, a 7000-Hz spectral width, and 64 or 80 scans per increment. For the evaluation of $^3J(H_NH_\alpha)$ values, 700 increments with 4K data points, and a 6000-Hz spectral width were acquired for the COSY experiment. Prior to Fourier transformation, all FIDs were multiplied by sine bell window functions, shifted by $\pi/16$ (unshifted for COSY). The final digital resolution was 6.88 Hz/point in both dimensions (TOCSY and NOESY) or 1.47 Hz/point in the t_2 dimension of the COSY experiment. Further data processing was performed on a Bruker Aspect X32 data station running under UNIX. Identification, location, and integration of the NOESY cross peaks was facilitated by the use of the program AURELIA (Neidig & Kalbitzer, 1990).

Structure Calculations. NOESY cross peaks were grouped into five categories based on their integrated intensities and calibrated against known distances in regular secondary structure elements resulting in upper distance limits of 0.25, 0.28, 0.32, 0.36, and 0.43 nm. Corrections for pseudoatoms were applied where necessary. Distance geometry calculations employing the program DISGEO (Havel & Wüthrich, 1984) were performed on a VAX 8600. Initial structures were created without embedding of intermediate substructures, and the metrization was replaced by filling in the initial distance matrix with uncorrelated random numbers between the geometric bounds.

The refinement of the distance geometry structures was accomplished by employing the GROMOS88 software package (van Gunsteren & Berendsen, 1987) on a Trace minisupercomputer (Multiflow Corp., Branford, CT). The NOEs were incorporated as upper limits for the distances between specific pairs of protons by using a semiharmonic extrapotential. The following protocol was used: 100 steps of unrestrained energy minimization were followed by another 500 steps with the distance restraints introduced with a force constant K_{dr} = 200 kJ·mol^{-1}·nm^{-2}. It was found that 3 ps of restrained molecular dynamics at a temperature of 300 K with the same force constant allowed the system to equilibrate. The dynamics continued at a temperature of 1000 K for 2 ps with K_{dr} = 1000 kJ·mol^{-1}·nm^{-2} and 10 ps with K_{dr} = 1500 kJ·mol^{-1}·nm^{-2}. Then the force constant was increased to its final value of 2000 kJ·mol^{-1}·nm^{-2} for 3 ps at 600 K and 32 ps at 300 K. The refinement was completed by 500 steps of restrained energy minimization. During the last 20 ps of the dynamics, trajectories were recorded for analysis of the structures. At temperatures above 300 K, the peptide bond torsion angles were additionally restrained by replacing their 2-fold potential minimum by a single one, with a force constant K_{dr} = 33.5 kJ·mol^{-1}. All calculations were performed "in vacuo" by employing the SHAKE algorithm with time steps of 0.001 ps.

The resulting structures were displayed on a Hewlett-Packard System 9000 with SRX graphics using the program BRAGI (Schomburg & Reichelt, 1988), which also allowed the calculation of the RMS deviations.

Results

Previous NMR investigations have shown that the human PTH fragment (1–34) does not adopt a well-defined tertiary structure in aqueous solution (Lee & Russell, 1989). In our own NMR investigations on the entire hormone (1–84), in the form of recombinant prolyl-hPTH(1–84), we reached the same conclusion, and this was confirmed by CD spectroscopic studies [for the preparation of the recombinant proly-hPTH(1–84), see Wingender et al. (1989)].

In contrast to these experimental results, the theoretical secondary structure prediction for human PTH implies the presence of two α-helical regions in the N-terminal part. CD spectra of the entire hormone indicative of a significant α-helical content could indeed be obtained after addition of trifluoroethanol (data not shown), well known to favor stabilization of secondary structure. This finding prompted us to investigate whether the same effect could be observed more directly by ^{1}H NMR studies on the fragment (1–34).

In a series of 1D NMR spectra acquired in D_2O, changes in the chemical shifts of α-protons and methyl groups were indeed found after addition of TFE-d_3 up to between 10 and 15% (v/v). Higher amounts, up to 50% (v/v), did not induce any further significant changes. This observation was confirmed by the 2D NOESY data in H_2O with 0, 5, 10, and 15% (v/v) TFE-d_3, where medium-range NOEs indicative of secondary structure were only present after addition of this reagent. As no alterations in the NOESY cross-peak intensities occurred between 10 and 15% (v/v) TFE-d_3, a full set

Table I: ^{1}H Assignment and Chemical Shift Data for hPTH Fragment (1–34) in 100 mM Phosphate Buffer and 10.7% TFE, pH 5.0, at 300 K

residue	NH	C^αH	C^βH	others
Ser 1		4.15	3.98	
Val 2	8.57	4.10	2.01	γH 0.89
Ser 3	8.26	4.37	3.94, 3.81	
Glu 4	8.51	3.95	1.99	γH 2.22
Ile 5	7.01	3.74	1.75	γH 1.45, 1.18; δH 0.76
Gln 6	7.78	3.96	2.08, 2.02	γH 2.30
Leu 7	7.69	4.03	1.63	γH 1.54; δH 0.78
Met 8	8.12	4.11	2.07	γH 2.44; γH 2.57
His 9	8.15	4.35	3.22	H2 8.43; H4 7.19
Asn 10	8.20	4.47	2.77, 2.81	
Leu 11	8.24	~4.11	~1.68	γH 1.49; δH 0.74
Gly 12	8.06	3.78, 3.67		
Lys 13	7.63	4.06	1.60	γ/δH 1.23; εH 2.85
His 14	8.04	4.52	3.19, 3.03	H2 8.39; H4 7.15
Leu 15	7.93	4.27	1.59	γH 1.44; δH 0.71
Asn 16	8.40	4.59	2.76, 2.89	
Ser 17	8.02	4.24	3.81, 3.93	
Met 18	8.27	4.25	2.02	γH 2.56; γH 2.46
Glu 19	8.36	4.02	1.94, 2.02	γH 2.32
Arg 20	7.97	4.06	1.85	γH 1.51; δH 3.04; εH 7.07
Val 21	7.66	3.66	2.14	γH 0.86; γH 0.98
Glu 22	8.05	4.00	2.06	γH 2.28
Trp 23	8.05	4.12	3.25, 3.39	H2 7.15; 3NH 10.01; H4 7.42; H5 6.91; H6 7.04; H7 7.33
Leu 24	8.03	3.72	1.65	γ/δH 0.82
Arg 25	8.25	3.74	1.79	γH 1.46; δH 3.01, 3.07; εH 7.30
Lys 26	7.65	3.90	1.73	γH 1.28; δH 1.43; εH 2.87
Lys 27	7.73	3.87	1.50	δH 141, 1.28; γH 0.81, 0.94; εH 2.61, 2.72
Leu 28	7.98	4.03	1.66	δH 0.71; γH 1.42
Gln 29	7.62	~4.05	2.02	γH 2.29; γH 2.37
Asp 30	7.80	4.52	2.69, 2.57	
Val 31	7.62	3.88	2.02	γH 0.76
His 32	8.24	4.53	3.09, 2.98	H2 8.44; H4 7.11
Asn 33	8.07	4.61	2.55, 2.64	
Phe 34	7.45	4.33	2.88, 3.04	ring-H ~7.4

of spectra were recorded with 10.7% (v/v) TFE-d_3. Similarly there was no change in the overall appearance of the NMR spectra with or without 100 mM phosphate buffer.

The amino acid spin systems were identified from a COSY experiment and used to establish direct J correlations between protons, and a CLEAN TOCSY spectrum was recorded with a mixing time of 80.7 ms in the fully protonated solvent mixture (Figure 1). This was completed by the same set of measurements conducted in the deuterated solvent. The well-established procedures based on short observable distances between H_N, H_α, and H_β of amino acid i and H_N of amino acid i+1, as manifested in the NOESY experiment, were used for the sequence specific assignment of the ^{1}H signals (Wüthrich, 1986). One starting point for establishing the residue positions in the peptide sequence was Trp 23, which was easily identified by several unique NOESY cross peaks between the protons of the indole ring system, its own H_N, and several protons of the adjacent Leu 24. Other entry points were the easily recognizable spin systems of Ser 3, Gly 12, and Ser 17. Figure 2 illustrates the sequence specific assignments for hPTH(1–34), showing the fingerprint region of a NOESY spectrum. Sequential d_{NN} connectivities are documented in Figure 3, and a list of the chemical shift values for the peptide fragment is given in Table I. A summary of the observed NOEs is shown in Figure 4. Besides sequential NOEs $d_{\alpha N}$ and d_{NN}, there are a number of medium-range NOEs $d_{\alpha_i N_{i+3}}$ and $d_{\alpha_i \beta_{i+3}}$ both between Val 2 and Asn 10 and between Ser 17 and Asp 29, indicating two α-helical segments. The sequence dependent $^3J(H_N-H_\alpha)$ values were estimated from the splittings, obtained from the well-digitized COSY spectrum, and further support this finding (Figure 5). No NOEs attributable to interactions of amino acid moieties more than four residues apart were observed.

A total of 133 distance restraints, derived from the NOESY spectrum with a mixing time of 250 ms, was used to calculate 104 distance geometry structures. It should be noted here that the upper distance limits corresponding to the observed $d_{\alpha N}$ NOEs had to be increased to give a satisfactory convergence. Fourteen DISGEO structures showed no more than one severe restraint violation in the range 0.1–0.12 nm and were selected for the subsequent molecular dynamics refinement. The nine best of these, as judged by their low potential and residual distance restraint energies, were subjected to the final analysis involving the placement and time course of hydrogen-bond formation. The energy values and RMS deviations are compiled in Table II, and the hydrogen-bond population data derived from the molecular dynamics calculations are given

Table II: Energy Values and RMS Deviations for the Final Nine Structures after Energy Minimization

structure no.	$E_{pot,tot}$[a] (kJ·mol^{-1})	E_{dr}[b] (kJ·mol^{-1})	RMS deviation[c] helix 1 (nm)	RMS deviation[c] helix 2[d] (nm)
1	−2369	26.6	0.069	0.117
2	−2104	42.2	0.102	0.113
3	−1898	65.9	0.088	0.219
4	−2383	39.8	0.095	0.126
5	−2437	23.1	0.083	0.103
6	−1050	83.3	0.094	0.215
7	−2722	62.0	0.120	0.119
8	−4562	42.1	0.102	0.114
9	−2376	46.5	0.098	0.105

[a] Total potential energy of the structure. [b] Residual distance restraint energy. [c] The RMS deviation for a particular structure was determined pairwise with each other structure to give eight values per structure. The average of these deviations is given. [d] Helix 1 is from Ser 3 to His 9 and helix 2 is from Ser 17 to Leu 28.

Table III: Hydrogen-Bond Data Averaged over the Final Nine Structures, with the Population Derived from Molecular Dynamics Calculations

hydrogen bonds		
donor	acceptor	pop. (%)
Ile 5–NH	Ser 3–CO	42.2
Gln 6–NH	Val 2–CO	86.7
Leu 7–NH	Ser 3–CO	50.0
Met 8–NH	Glu 4–CO	58.9
His 9–NH	Ile 5–CO	85.6
Asn 10–NH	Gln 6–CO	65.6
Leu 11–NH	Leu 7–CO	43.3
Gly 12–NH	His 9–CO	27.8
Lys 13–NH	His 9–CO	53.3
His 14–NH	Gly 12–CO	21.1
Leu 15–NH	Lys 13–CO	27.8
Asn 16–NH	His 14–CO	37.8
Ser 17–NH	Leu 15–CO	36.7
Met 18–NH	Asn 16–CO	33.3
Arg 20–NH	Ser 17–CO	21.1
Val 21–NH	Ser 17–CO	72.2
Glu 22–NH	Met 18–CO	75.6
Trp 23–NH	Glu 19–CO	65.6
Leu 24–NH	Arg 20–CO	77.8
Arg 25–NH	Val 21–CO	94.4
Lys 26–NH	Glu 22–CO	91.1
Lys 27–NH	Trp 23–CO	67.8
Leu 28–NH	Leu 24–CO	71.1
Gln 29–NH	Arg 25–CO	32.2
Val 31–NH	Gln 29–CO	23.3
His 32–NH	Asp 30–CO	22.2
Phe 34–NH	His 32–CO	44.4

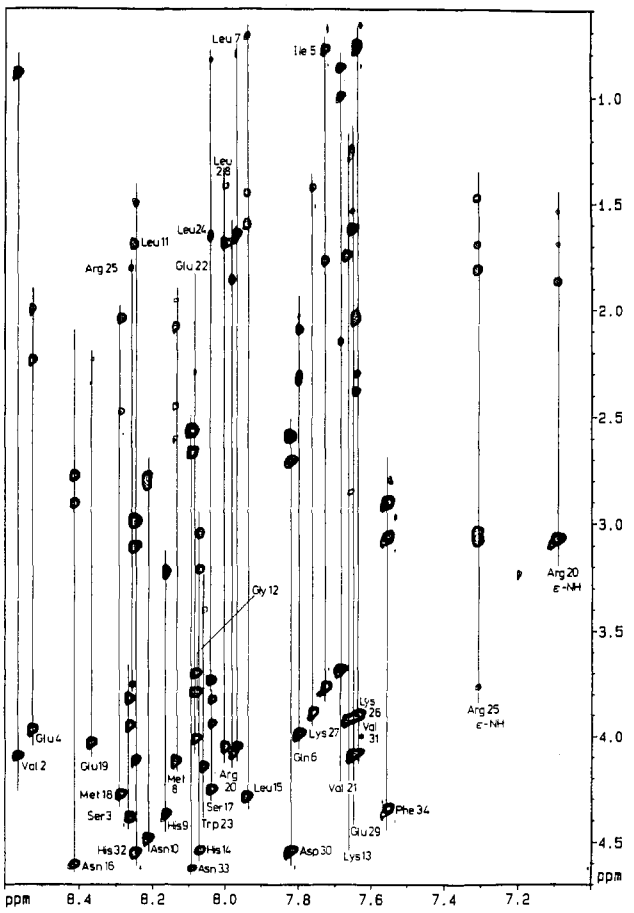

FIGURE 1: Part of a 2D CLEAN TOCSY spectrum (mixing time 80.7 ms) of hPTH(1–34) in 100 mM phosphate buffer in 10.7% (v/v) TFE-d_3, pH 5.0, showing all amino acid spin systems.

in Table III. The averaged backbone angles ϕ and ψ are given in Figure 7.

Discussion

The experimental results presented here give the first unequivocal evidence that, under certain solution conditions, parts of the human PTH fragment (1–34) adopt defined helical structures. The family of structures, derived from NMR spectroscopy and restrained molecular dynamics simulations, correspond remarkably well with the theoretically predicted secondary structure as can be seen in the comparison of Figure 4 with Figure 6. The RMS deviations among the energy-minimized final structures are low from Ser 3 to His 9 and again from Ser 17 to Leu 28, and, together with the hydrogen-bond data, imply two α-helices confined to these regions. As expected the N and C termini are flexible, and a distinct nonordered linker region is evident that connects the helices. The latter does not allow a discrimination among the various relative orientations of the two structured regions (Figure 8).

Basically the existence of two helices, which have previously been suggested mainly from theoretical considerations (Fiskin et al., 1977; Zull et al., 1980), is confirmed. Careful inspection of the NOE data (Figure 4) shows that the intensities of the sequential $d_{\alpha N}$ NOEs compared to the d_{NN} NOEs are stronger than expected for an ideal stable helix. This can be attributed to the occurrence of a dynamic equilibrium between helical and nonhelical structures. Taking this into account, it can be concluded from the NOE intensities that on average the helices are the predominant structural features in these regions under the solvent conditions applied in this study. A similar consideration explains the overall tendency of the J coupling

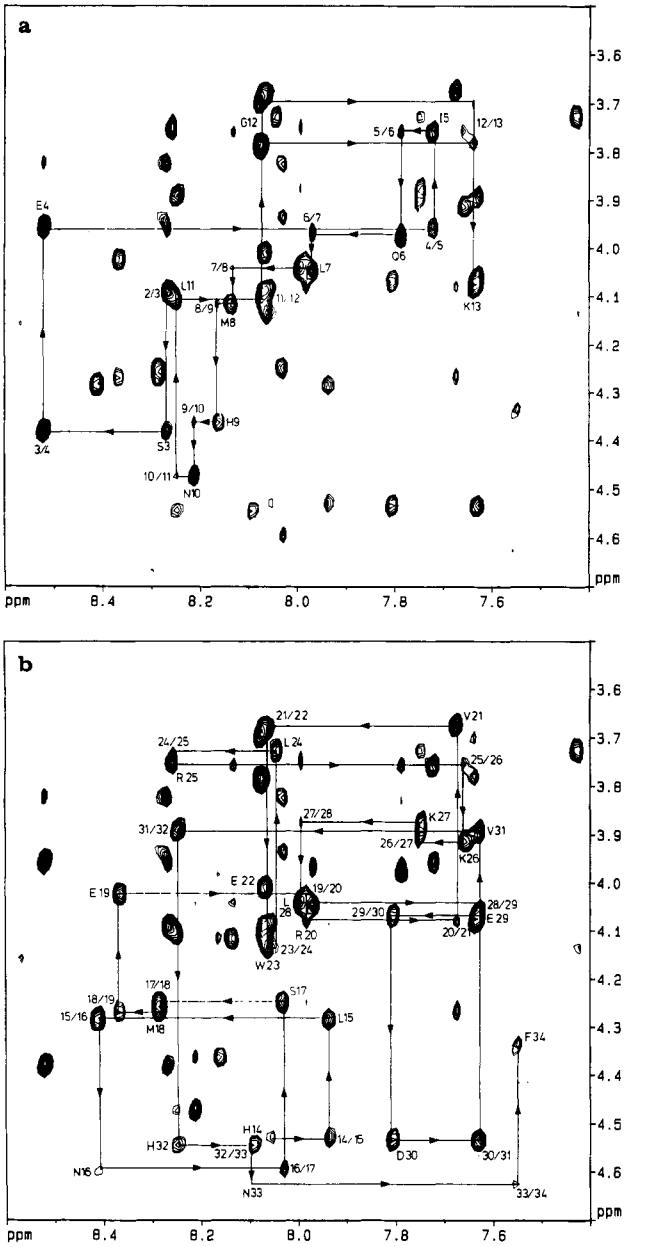

FIGURE 2: Fingerprint region of the 2D NOESY spectrum (mixing time 250 ms) of hPTH(1–34) showing the sequential assignments of the peptide [(a) S3 to K13; (b) H14 to F34]. For the solution conditions see the legend to Figure 1.

constants to be higher than expected for an ideal helix. The J values from Arg 20 to Glu 22 imply an even higher local flexibility in this part of the second helix. The absence of helical structure in the linker region might explain the exceptional coupling constant of Gly 12 (see Figure 5).

Further confirmation of the general structural features is also apparent from the average values of the ϕ and ψ backbone angles and their RMS deviations. A defined β-turn at Gly 12 and Lys 13 has been postulated by secondary structure prediction programs and was proposed by NMR studies with the N-terminal fragment of PTH-related peptide (Barden & Kemp, 1989). However, the absence of any medium-range NOEs in this linker region of hPTH(1–34) indicates that a stable turn is not preferred under these solution conditions. Various implications regarding the relationship between the present three-dimensional structures and the biological activities can be deduced from these findings. The linkage between the two helices by a flexible region rather than a β-turn

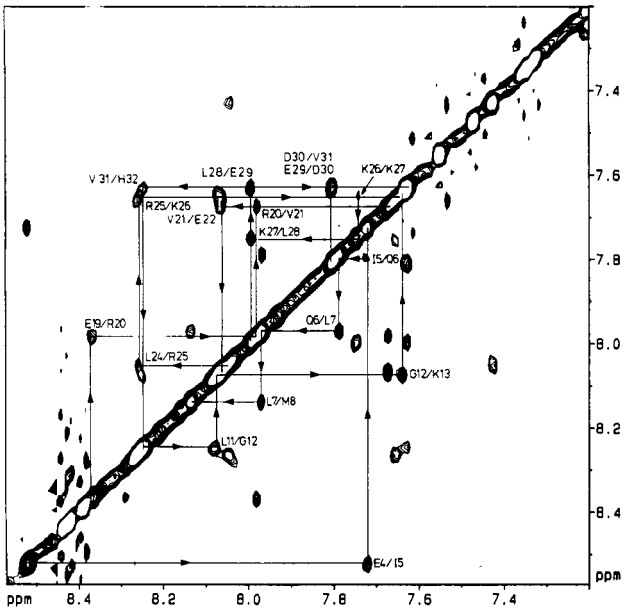

FIGURE 3: 2D NOESY spectrum (same spectrum as in Figure 2) showing the d_{NN} connectivities.

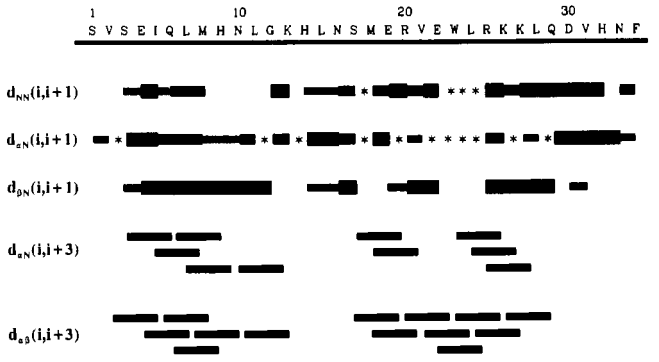

FIGURE 4: Summary of the observed NOEs for hPTH(1–34) (For solution conditions see the legend to Figure 1).

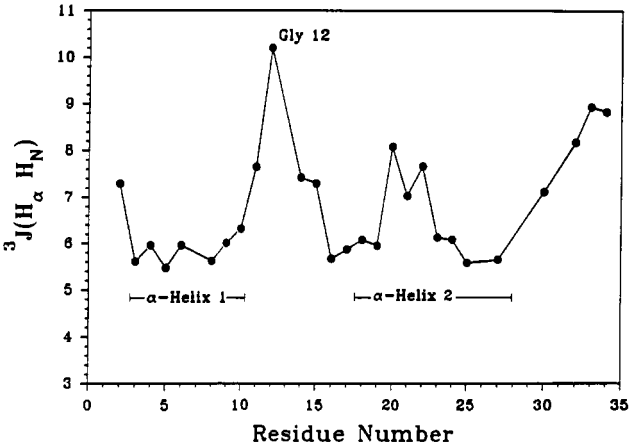

FIGURE 5: Sequence specific vicinal $J(H_\alpha-H_N)$ values for hPTH(1–34) estimated from the splittings from a well-digitized COSY spectrum.

coincides with the loss of hormonal activity in an in vitro adenylate cyclase assay after either a Gly12Pro or a Lys13Pro substitution whereas exchanges by Ala in position 12 or by Leu or Ser in position 13 retain the activity [Chorev et al. (1990) and Wingender et al. (unpublished results)]. This flexible linker allows the two helical domains to be arranged such that the formation of a salt bridge between Glu 4 and Arg 20 is possible. Position 20 in the PTH sequence seems to be of considerable importance for the functions of the

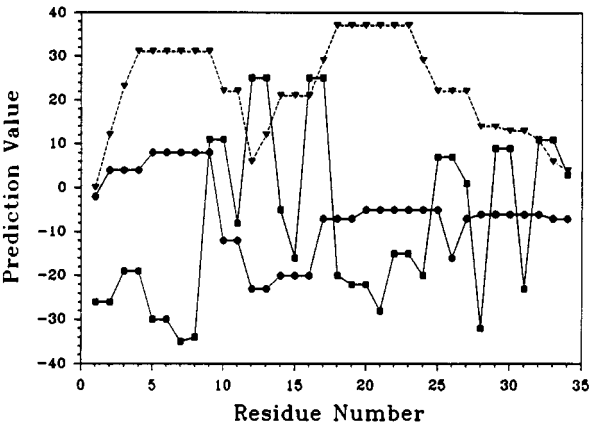

FIGURE 6: Prediction of secondary structural elements according to the algorithm of Garnier et al. (1978). Symbols: (■) β-turn, (●) extended, and (▼) α-Helix.

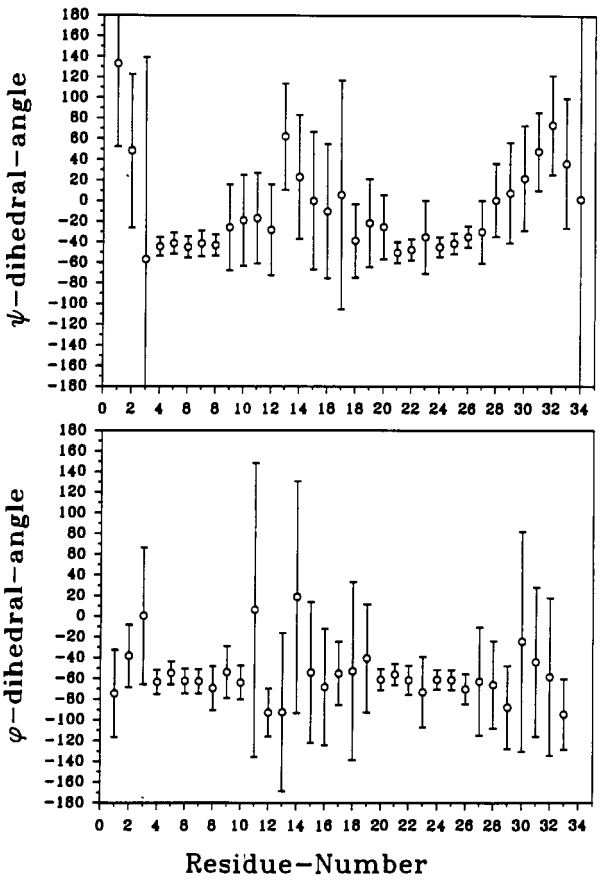

FIGURE 7: Backbone angles ϕ and ψ averaged over MD trajectories each of 20-ps duration of the nine final structures. The length of the vertical bars indicates the rms deviation.

hormone as the amino acid exchange of Arg for Glu causes loss of complete hormonal activity [Wingender et al. (unpublished results)]. This might be explained by the disruption of the postulated salt bridge or by the fact that the introduction of this amino acid, which has the highest helix-forming potential, diminishes the flexibility in this region, thereby stabilizing the helix and resulting in a structure that may be too rigid to interact with the corresponding receptor.

Thus for the amino-terminal fragment (1–34) of the PTH molecule, there are three levels of flexibility that must be considered. These are (1) the overall flexibility of the PTH molecule in solution, which can be influenced by trifluoroethanol, (2) the potential flexibility within the second α-helix, and (3) the high flexibility in the linker region between the

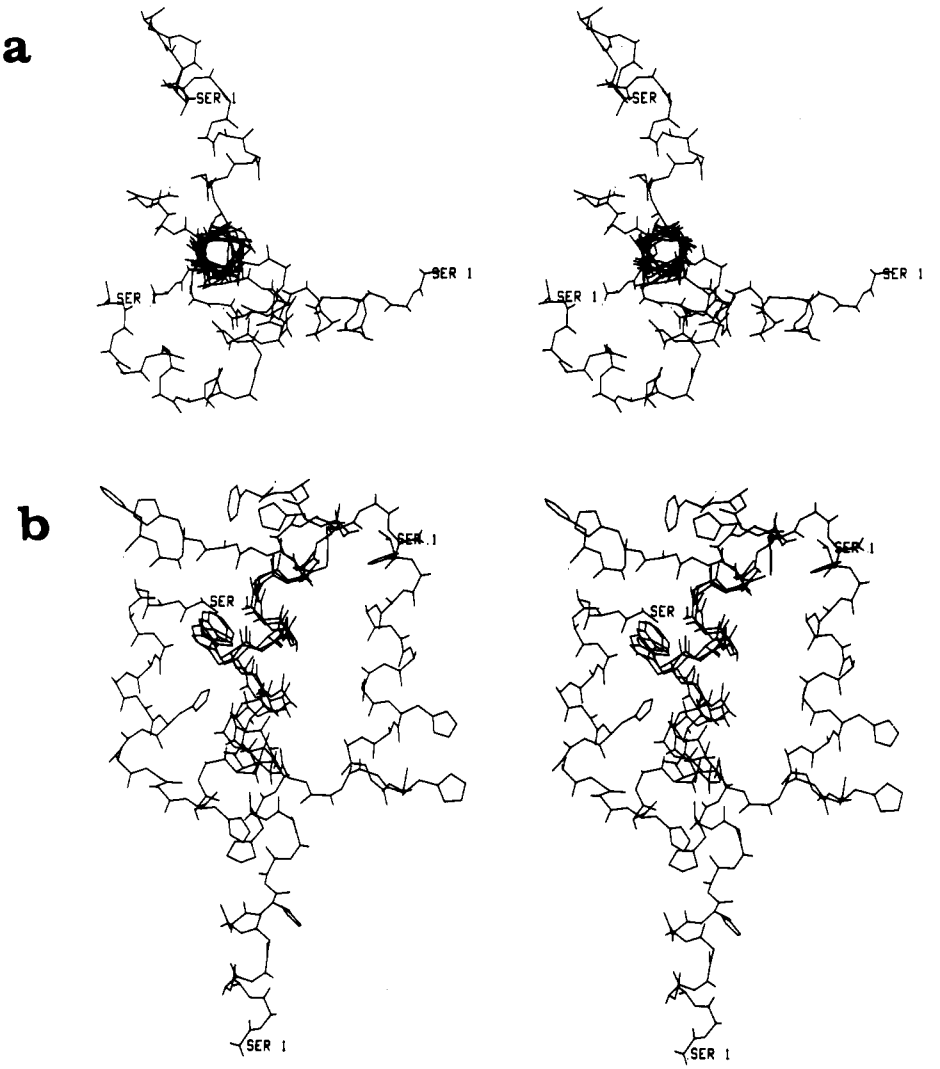

FIGURE 8: (a) Stereoview of three final MD structures aligned for minimal rms deviation within the second helix S17 to L28. Viewed along the helix axis. (b) Stereoview of three other final MD structures with same alignment as in panel a viewed parallel to the helix axis.

helices. This property of the PTH molecule may also be of biological significance, since it has been shown that two different functional domains of PTH trigger either cAMP-dependent or -independent cellular responses. Conceivably, there may exist different PTH receptor (sub)types (Löwik et al., 1985; Dunlay et al., 1990). At least one of these, the one being connected to the adenylate cyclase system, interacts with the PTH region 14–34, which comprises part of the highly flexible linker region and the second helix (Caulfield et al., 1990), and this receptor recognition site seems to exhibit a bipartite structure (Potts et al., 1982). However, binding to another receptor might involve different structural features, and therefore the ability of one molecule to interact with different receptor (sub)types might require a considerable degree of flexibility of the ligand. Nevertheless, during binding to the receptor, the hormone may adopt a defined structure or one of several alternative structures depending on the receptor (sub)type. It seems likely that the solvent mixture used in this study has mimicked an environment similar to that found in the vicinity of the receptor. Preliminary NMR studies in a 10% SDS micelle solution show the presence of at least five slowly exchanging amide protons indicating their participation in more stable hydrogen bonds and hence the existence of a less flexible secondary structure under these conditions. Structural information elucidated in this work will serve as a guideline for structural investigation of the whole protein. Moreover, it also provides a basis for the generation of PTH mutants with altered structural and functional properties.

Registry No. PTH, 52232-67-4.

REFERENCES

Barden, J. A., & Kemp, B. E. (1989) *Eur. J. Biochem. 184*, 379–394.

Bax, A., & Davis, D. G. (1985) *J. Magn. Reson. 65*, 355–360.

Bundi, A., Andreatta, R., Rittel, W., & Wüthrich, K. (1976) *FEBS Lett. 64*, 126–129.

Bundi, A., Andreatta, R. H., & Wüthrich, K. (1978) *Eur. J. Biochem. 91*, 201–208.

Caulfield, M. P., McKee, R. L., Goldman, M. E., Duong, L. T., Fisher, J. E., Gay, C. T., DeHaven, P. A., Levy, J. J., Roubini, E., Nutt, R. F., Chorev, M., & Rosenblatt, M. (1990) *Endocrinology 127*, 83–87.

Chorev, M., Goldman, M. E., McKee, R. L., Roubini, E., Levy, J. J., Gay, C. T., Reagan, J. E., Fisher, J. E., Caporale, L. H., Golub, E. E., Caulfield, M. P., Nutt, R. F., & Rosenblatt, M. (1990) *Biochemistry 29*, 1580–1586.

Coddington, J. M., & Barling, P. M. (1989) *Mol. Endocrinol. 3*, 749–753.

Davis, D. G., & Bax, A. (1985) *J. Am. Chem. Soc. 107*, 2820–2821.

Dewhirst, F. E., Ago, J. M., & Stashenko, P. (1990) *Calcif. Tissue Int. 47*, 1–7.

Dunlay, R., Civitelli, R., Miyauchi, A., Dobre, C. V., Gupta, A., Goligorsky, M., & Hruska, K. (1990) *Calcium Regulation and Bone Metabolism 10* (Cohn, D. V., Glorieux, F. H., & Martin, T. J., Eds.) pp 24-32, Excerpta Medica, Amsterdam-New York-Oxford.
Fiskin, A. M., Cohn, D. V., & Peterson, G. C. (1977) *J. Biol. Chem. 252*, 8261-8268.
Garnier, J., Osguthorpe, D. J., & Robson, B. (1978) *J. Mol. Biol. 120*, 97-120.
Griesinger, C., Otting, G., Wüthrich, K., & Ernst, R. R. (1988) *J. Am. Chem. Soc. 110*, 7870-7872.
Havel, T. F., & Wüthrich, K. (1984) *Bull. Math. Biol. 46*, 673-698.
Herrmann-Erlee, M. P. M., van der Meer, J. M., Löwik, C. W. G. M., van Leeuwen, J. P. T. M., & Boonekamp, P. M. (1988) *Bone 9*, 93-100.
Jeener, J., Meier, B. H., Bachmann, P., & Ernst, R. R. (1979) *J. Chem. Phys. 71*, 4546-4553.
Lee, S. C., & Russell, A. F. (1989) *Biopolymers 28*, 1115-1127.
Lincoln, D. N., Graf, G., Leuner, U., Lehnberg, W., & Blöcker, H. (1990) GENMON User Manual, GBF, Braunschweig, Germany.
Löwik, C. W. G. M., van Leeuwen, J. P. T. M., van der Meer, J. M., van Zeeland, J. K., Scheven, B. A. A., & Herrmann-Erlee, M. P. M. (1985) *Cell Calcium 6*, 311-326.
Macura, S., Huang, Y., Sutter, D., & Ernst, R. R. (1981) *J. Magn. Reson. 43*, 259-281.
Marion, D., & Wüthrich, K. (1983) *Biochem. Biophys. Res. Commun. 113*, 967-974.
Martz, A., & Thomas, M. L. (1983) *Biochem. Pharmacol. 32*, 3429-3433.
Neidig, K.-P., & Kalbitzer, H. R. (1990) *J. Magn. Reson. 88*, 155-160.
Potts, J. T., Jr., Kronenberg, H. M., & Rosenblatt, M. (1982) *Adv. Protein Chem. 35*, 323-396.
Rance, M., Sorensen, O. W., Bodenhausen, G., Wagner, G., Ernst, R. R., & Wüthrich, K. (1983) *Biochem. Biophys. Res. Commun. 117*, 479-485.
Redfield, A., & Kunz, S. D. (1975) *J. Magn. Reson. 19*, 250-254.
Schlüter, K.-D., Hellstern, H., Wingender, E., & Mayer, H. (1989) *J. Biol. Chem. 264*, 11087-11092.
Schomburg, D., & Reichelt, J. (1988) *J. Mol. Graphics 6*, 161-165.
Smith, L. M., Jentoft, J., & Zull, J. E. (1987) *Arch. Biochem. Biophys. 253*, 81-86.
Sömjen, D., Bindermann, I., Schlüter, K.-D., Wingender, E., Mayer, H., & Kaye, A. M. (1990) *Biochem. J. 272*, 781-785.
Sömjen, D., Schlüter, K.-A., Wingender, E., Mayer, H., & Kaye, A. M. (1991) *Biochem. J.* (in press).
van Gunsteren, W. F., & Berendsen, H. J. C. (1987) GROMOS Manual, Biomos, Groningen.
Wingender, E., Bercz, G., Blöcker, H., Frank, R., & Mayer, H. (1989) *J. Biol. Chem. 264*, 4367-4373.
Wüthrich, K. (1986) *NMR of Proteins and Nucleic Acids*, J. Wiley & Sons, New York.
Zuiderweg, E. R. P., Hallenga, K., & Olejniczak, E. T. (1986) *J. Magn. Reson. 70*, 336-343.
Zull, J. E., & Lev, N. (1980) *Proc. Natl. Acad. Sci. U.S.A. 71*, 3791-3796.
Zull, J. E., Smith, L. M., Chuang, J., & Jentoft, J. (1987) *Mol. Cell. Endocrinol. 51*, 267-271.

Photodependent Inhibition of Rat Liver NAD(P)H:Quinone Acceptor Oxidoreductase by (A)-2-Azido-NAD$^+$ and (A)-8-Azido-NAD$^+$†

Paulis S. K. Deng,‡ Sui-Hung Zhao,‡ Takashi Iyanagi,§ and Shiuan Chen*,‡
Division of Immunology, Beckman Research Institute of the City of Hope, Duarte, California 91010, and Department of Biochemistry, University of Tsukuba, Niihari-gun, Ibaraki-ken, 305 Japan
Received January 30, 1991; Revised Manuscript Received March 20, 1991

ABSTRACT: Two photoaffinity analogues of NAD$^+$, (A)-2-azido-NAD$^+$ [nicotinamide 2-azidoadenine dinucleotide] and (A)-8-azido-NAD$^+$ [nicotinamide 8-azidoadenine dinucleotide], have been synthesized, and their reactivities with the rat liver NAD(P)H:quinone acceptor oxidoreductase have been investigated. The reduce nicotinamide nucleotide probes, (A)-2-azido-NADH and (A)-8-azido-NADH, were shown to be substrates of the quinone reductase. This enzyme was inhibited by (A)-2-azido-NAD$^+$ and (A)-8-azido-NAD$^+$ in a photodependent manner, and the inhibition of the enzyme could be prevented by the presence of nicotinamide nucleotide substrates during photolysis. (A)-2-Azido-NAD$^+$ was demonstrated to be a more potent inhibitor than (A)-8-azido-NAD$^+$. In addition, the photodependent inhibition by (A)-8-azido-NAD$^+$ increased when menadione, the substrate of the enzyme, was present during the photolysis, while menadione protected the enzyme from the photodependent inhibition by (A)-2-azido-NAD$^+$. These results indicate that these two NAD$^+$ analogues can be used to identify the nicotinamide nucleotide binding site of this quinone reductase and that they probably bind to the enzyme in different fashions.

NAD(P)H:quinone acceptor oxidoreductase(EC 1.6.99.2; DT-diaphorase) plays an important role in protecting tissues against the mutagenic, carcinogenic, and cytotoxic effects of quinones that occur widely in nature (Ernster, 1987). Protection is accomplished by the unique property of this quinone reductase to catalyze an obligatory two-electron reduction of several quinones, including vitamin K (e.g., menadione), to hydroquinones with either NADH or NADPH as electron donor (Iyanagi & Yamazaki, 1970; Iyanagi, 1987). This

† This research was supported by NIH Grants GM37297 and 33572.
* Correspondence should be addressed to this author.
‡ Beckman Research Institute of the City of Hope.
§ University of Tsukuba.

0006-2960/91/0430-6942$02.50/0